




Lead Green's functions from quadratic eigenvalue problems without mode velocity calculations

Gunnar Thorgilsson  and Sigurdur I. Erlingsson ^{*}

Department of Engineering, Reykjavik University, Menntavegi 1, IS-102 Reykjavik, Iceland

 (Received 1 February 2023; accepted 13 October 2023; published 13 November 2023)

In quantum transport calculations, the proper handling of incoming and outgoing modes for retarded Green's functions is achieved via the lead self-energies. Computationally efficient and accurate methods to calculate the self-energies are thus very important. Here we present an alternative method for calculating lead self-energies which improves on a standard approach to solving quadratic eigenvalue problems that arise in quantum transport modeling. The method is based on a perturbative analysis of the generalized Schur decomposition to determine the relevant set of eigenvalues for transmitting modes. This allows us to circumvent finding the velocities of the modes (left- or right-moving) that are needed in order to calculate the lead Green's function from translationally invariant Green's functions. This saves computational time irrespective of the value of the imaginary part added to the energy. We compare our method with two existing methods—a popular iterative method and a standard eigenvalue method that explicitly calculates the velocities of the propagating modes. Our comparison shows that both eigenvalue methods are more robust than the iterative method. Furthermore, the comparison also shows that above a small threshold of propagating modes, the standard eigenvalue method requires extra computation time over our perturbation method. This excess of computation time grows linearly with the number of propagating modes.

DOI: [10.1103/PhysRevE.108.055304](https://doi.org/10.1103/PhysRevE.108.055304)

I. INTRODUCTION

A central quantity in quantum transport calculations are the lead self-energies [1,2]. The self-energies play the role of representing the asymptotic behavior of the system, which in traditional scattering theory is composed of outgoing and incoming wave solutions [3]. In the context of quantum transport, the system under study is defined as the central part, or scattering area, that determines the propagation through the system, but the properties of the incoming and outgoing modes are encoded in the self-energies [2]. In the usual language of quantum transport, the region of space connecting the scattering area to infinity is called the leads [4,5]. The self-energies are related to the Green's functions of the leads, which we will define in detail later. Once the leads are attached to the scattering area, particles within the scattering area can leak out, i.e., the states will acquire a finite lifetime. The lifetime, and energy shift, due to the leads can be extracted from the imaginary, and real, part of the self-energies, respectively [6]. The self-energies are in general complex-valued, even though the underlying Hamiltonians are Hermitian and thus have real eigenenergies.

The self-energies are determined by the Green's functions (GFs) of the leads, often referred to as the surface GF. They can be solved analytically for some simple cases where the transverse and longitudinal directions are decoupled [2] or when the matrices involved are small [7,8], but in general they have to be calculated numerically. The methods to calculate the lead Green's function can be separated into two

categories: (i) iterative methods and (ii) eigenvalue methods. The work horse of the iterative method, introduced by Lopez-Sancho *et al.*, calculates the surface GF using a decimation method [9].

The eigenvalue method in connection with quantum transport can be traced back to Ando [10], where a quadratic eigenvalue problem was solved. The concept of *removal invariance* was used to derive self-consistent equations for surface Green's functions [11] and also to derive quadratic equations for the Green's function [12]. The same quadratic eigenvalue problem was formulated by Dy, Wu, and Spratlin [13]. This method has also been applied to *ab initio* computational problems [14–16]. The method has been explained in detail [17,18] and applied to numerous system [19–24]. The wave-function method [25] is related to the eigenvalue method of finding the surface Green's functions [26].

In the eigenvalue method [14–17,19–21,27], the GF of the half-infinite lead is obtained from the infinite system, where Bloch's theorem can be used. Converting the Bloch form to the surface GF requires knowledge of the velocity of the propagating modes, which have to be calculated separately to identify which eigenvalues to use [18]. It was even pointed out that a crucial step in the derivation may break down if two propagating modes have zero velocity, although this seems not to be a critical point for most realistic systems [18].

In this work, we will present an alternative, efficient, way to determine which eigenvalues to use for solving the quadratic eigenvalue problem *without* having to find the velocities of the propagating modes. Our method follows the standard way of solving the quadratic eigenvalue problem, but we will use at the level of the generalized Schur decomposition (GSD) a perturbation analysis to select which eigenvalues to use, thus

^{*}sie@ru.is

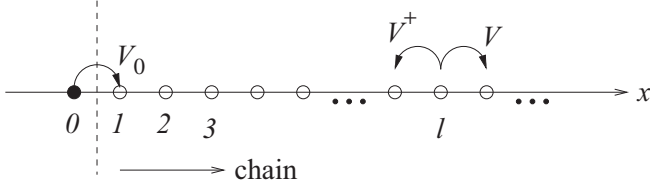


FIG. 1. A half-infinite chain with sites $l = 1, 2, 3, \dots$ where each site is described by a matrix H and coupling $V(V^\dagger)$ to the right (left) side neighbor. An additional site is described by H_0 and coupling V_0 , and if $H_0 = H$ and $V_0 = V$, then the Green's function on site 1 and 0 should be the same.

bypassing the velocity-finding part. The present method can be used for any algorithm using GSD, such as for order N methods [28], and also wave mode decomposition [29].

The paper is organized as follows. To clarify the underlying concepts, a review of the standard quadratic method for calculating self-energies is presented in Sec. II. In Sec. III, we outline the standard solution approach, i.e., the GSD, for the eigenvalue problem, and we introduce our method of eigenvalue selection. In the final section, we consider two test cases in which we compare our method with the standard eigenvalue method and the iterative method.

II. GENERAL SELF-ENERGY MODEL

Our starting point is a general tight-binding model represented in Fig. 1, which shows a half-infinite chain with sites labeled $l = 1, 2, \dots$ and all sites represented by a Hermitian matrix H . The coupling between sites l and $l + 1$ is given by the matrix V and, correspondingly, V^\dagger describes the coupling between sites l and $l - 1$. The matrices V and H have the same dimension $N \times N$, where N can represent, e.g., the number of transverse points in a 2D or 3D system [15,20], spin, or any other internal degree of freedom, e.g., spd-orbitals [14–16]. The Green's function for the chain (sites $l \geq 1$) is denoted by \mathbb{G}_c . The quantity of interest is the Green's function for site $l = 1$, i.e., $[\mathbb{G}_c]_{1,1} \equiv G_{1,1}$, sometimes called the surface Green's function. If a new site $l = 0$ is attached to the chain, with on-site matrix H_0 and coupling matrix V_0 that describes the coupling between $l = 0$ and 1, the Green's function of site $l = 0$ is given by

$$G_{0,0} = (E - H_0 - V_0 G_{1,1} V_0^\dagger)^{-1}; \quad (1)$$

see Appendix A for a detailed derivation. Note that the self-energy due to the chain is defined as

$$\Sigma_c = V_0 [\mathbb{G}_c]_{1,1} V_0^\dagger. \quad (2)$$

If site $l = 0$ is identical to the other $l > 0$ sites, i.e., $H_0 = H$ and $V_0 = V$, then the chain is again a half-infinite chain with identical on-site matrices H and couplings V and thus we have that $G_{0,0} = [\mathbb{G}_c]_{1,1} \equiv G$, and the equation for the surface Green's function, G , is then

$$G = (E - H - V G V^\dagger)^{-1}, \quad (3)$$

which reduces to a quadratic matrix equation

$$(E - H)G - V G V^\dagger G = \mathbb{I}. \quad (4)$$

Note that Eq. (4) is valid for any V or H , and specifically V can be rank-deficient. For completeness, we point out that the Green's function in Eq. (4) would correspond to the (R)ight Green's function G_R , and the corresponding equation for the (L)eft Green's function would be

$$(E - H)G_L - V^\dagger G_L V G_L = \mathbb{I}, \quad (5)$$

which is structurally the same quadratic equation, the only difference being the interchange of V and V^\dagger .

Equation (4) is a common starting point when calculating the surface Green's function. It is important, however, to keep in mind that Eq. (4) is derived from an infinite matrix equation, whose solution relied on summing a geometric series of the eigenvalues [13]. The series only converge when the eigenvalues lie on or within the unit circle in the complex plane [13]. This places a natural condition on the physically relevant eigenvalues, which allows us to use efficient means to calculate the Green's functions.

Our goal is to directly solve this quadratic equation without having to find the Green's function of the infinite system using translational invariance [17,18]. To construct the surface Green's function from the translationally invariant one, the transmitting states on the unit circle have to be identified and separated into left-moving and right-moving states [18]. This in turn requires additional computation time that grows linearly with the number of eigenvalues on the unit circle, i.e., the number of transmitting states, which the current method bypasses.

Equation (4) can be transformed into a standard quadratic equation by right-multiplying with V^\dagger , which results in

$$V(GV^\dagger)^2 - (E - H)(GV^\dagger) + V^\dagger = 0. \quad (6)$$

This equation is the starting point of our analysis. Assuming that GV^\dagger is diagonalizable, then it can be written as

$$GV^\dagger = U_{<} \Lambda_{<} U_{<}^{-1}, \quad (7)$$

where $\Lambda_{<} = \text{diag}\{\lambda_n\}$ is a diagonal matrix containing the eigenvalues, and $U_{<}$ contains the eigenvectors as columns vectors [30]. The $<$ subscript is used here to emphasize that the eigenvalues should fulfill $|\lambda_n| < 1$ [13,31]. Indeed, the intersite Green's function $G_{n,0}$ can be written as (see Appendix B)

$$G_{n,0} V^\dagger = (G_{0,0} V^\dagger)^{n+1} \quad (8)$$

$$= U_{<} \Lambda_{<}^{n+1} U_{<}^{-1}, \quad (9)$$

which highlights that eigenvalues $|\lambda_n| > 1$ would lead to diverging solutions as a function of the intersite distance.

The remaining task is to find the eigenvalues and vectors in Eq. (7). Inserting Eq. (7) into (6) and right-multiplying with $U_{<}$ results in

$$V U_{<} \Lambda_{<}^2 - (E - H) U_{<} \Lambda_{<} + V^\dagger U_{<} = 0. \quad (10)$$

The n th column ($n = 1, 2, \dots, N$) of the matrix in Eq. (10) is given by

$$(V \lambda_n^2 - (E - H) \lambda_n + V^\dagger) \mathbf{x}_n = \mathbf{0}, \quad (11)$$

since $U_{<} = [\mathbf{x}_1, \mathbf{x}_2, \dots, \mathbf{x}_N]$, where \mathbf{x}_n is a column eigenvector corresponding to eigenvalue λ_n [30]. This is a quadratic eigenvalue problem that our aim is to solve. We can obtain useful information about the eigenvalues λ_n by studying

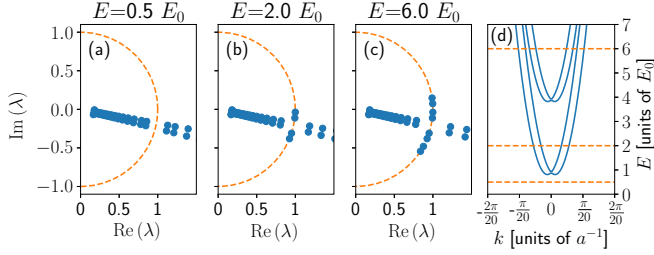


FIG. 2. Eigenvalues for the Schrödinger equation solved for a two-dimensional wire with Rashba spin-orbit interaction as described in Sec. IV with side length L_y . The energy E is measured in the hopping parameter t and momentum k in inverse grid spacing a^{-1} . The dimension of the matrices V and H is $N = 50$. Parts (a)–(c) show the $2N$ eigenvalues of the quadratic eigenvalue problem for (a) $E = 0.5E_0$, (b) $E = 2E_0$, and (c) $E = 6E_0$. Part (d) shows the corresponding dispersion energies as a function of k , with the dashed lines indicating $E = 0.5E_0$, $2.0E_0$, and $6.0E_0$ showing the number of propagating modes: (a) $E = 0.5E_0$ has no propagating modes, (b) $E = 2E_0$ has four propagating modes, and (c) $E = 6E_0$ has eight propagating modes.

the properties of Eq. (6). By right-multiplying Eq. (6) by $(GV^\dagger)^{-2}U$ and taking the Hermitian conjugate, one obtains

$$U^\dagger V^\dagger - ((\Lambda^*)^{-1})U^\dagger(E - H) + ((\Lambda^*)^{-1})^2 U^\dagger V = 0. \quad (12)$$

Each line of the above equation is of the form

$$\mathbf{x}_n^\dagger (V(1/\lambda_n^*)^2 - (E - H)(1/\lambda_n^*) + V^\dagger) = \mathbf{0}, \quad (13)$$

which shows, by comparison of Eqs. (11) and (13), that the eigenvalues come in pairs $(\lambda_n, 1/\lambda_n^*)$. This result can be obtained by looking at the characteristic polynomial [13]. This means that it can be hard to distinguish between eigenvalues in a given pair when they are close to the unit circle. For eigenvalues on the unit circle, $\lambda_n = e^{i\theta_n} = 1/\lambda_n^*$, and only by adding an imaginary part to E can they be distinguished, i.e., which of the eigenvalues of the pair to keep in Eq. (7) [13]. This behavior can be seen in Fig. 2, which shows the eigenvalues for the Schrödinger equation solved on a two-dimensional strip in the presence of spin-orbit interaction and a perpendicular magnetic field [32,33]. The magnetic field is used here to illustrate that the distribution of eigenvalues λ does not have to be symmetric around the real axis. The value of the magnetic field B is set by the ratio $\ell_c/L_y = 0.3$, where $\ell_c = \sqrt{\hbar}/eB$ is the magnetic length. The details of the model will be discussed in Sec. IV and Appendix C. Figure 2 shows the eigenvalues for energies E/E_0 (a) 0.5, (b) 2.0, and (c) 6.0 for a two-dimensional wire with Rashba spin-orbit interaction as described in Sec. IV. The number of eigenvalues lying on the unit circle corresponds to the number of propagating modes as seen in Fig. 2(d), where $E/E_0 = 0.5$, 2.0, and 6.0 have zero, four, and eight intersection points, respectively, with the dispersion curves. Note that when counting the number of intersection points, one has to account for spin (doubling of eigenvalues).

III. SOLVING THE EIGENVALUE PROBLEM

The standard way of solving quadratic eigenvalue problems is to linearize the quadratic problem [30]. Since our method of choosing the proper subset of eigenvalues relies on the specific structure of the matrices and also the details of the GSD [30,34], we will outline it here for completeness. The quadratic eigenvalue problem in Eq. (11) can be rewritten into the standard linear, generalized eigenvalue problem by introducing a new vector $\mathbf{u} = (\mathbf{x}, \lambda\mathbf{x})^T$. This leads to a linear problem with matrices twice the size,

$$\lambda \begin{pmatrix} 1 & 0 \\ 0 & V \end{pmatrix} \begin{pmatrix} \mathbf{x} \\ \lambda\mathbf{x} \end{pmatrix} - \begin{pmatrix} 0 & 1 \\ -V^\dagger & [(E + i\eta) - H] \end{pmatrix} \begin{pmatrix} \mathbf{x} \\ \lambda\mathbf{x} \end{pmatrix} = \begin{pmatrix} \mathbf{0} \\ \mathbf{0} \end{pmatrix}, \quad (14)$$

where we have introduced a *positive* infinitesimal imaginary part $i\eta$ to E , where $\eta = 0^+$. This ensures that the resulting GF is retarded, and for a *negative* infinitesimal imaginary part the advanced GF is obtained. Equation (14) can be written more concisely as

$$\lambda B\mathbf{u} - A\mathbf{u} = 0, \quad (15)$$

where the matrices A and B are defined as

$$A = \begin{pmatrix} 0 & 1 \\ -V^\dagger & [(E + i\eta) - H] \end{pmatrix} = A_0 + i\eta \begin{pmatrix} 0 & 0 \\ 0 & \mathbb{I} \end{pmatrix}, \quad (16)$$

where the matrix A_0 is defined at the value of A at $\eta = 0$ and

$$B = B_0 = \begin{pmatrix} 1 & 0 \\ 0 & V \end{pmatrix}, \quad (17)$$

where $B = B_0$ since η does not appear in B . Note that B can be singular if V is rank-deficient, which naturally occurs in, e.g., graphene nanoribbons [35,36]. As was discussed above, only the eigenvalues with $|\lambda| \leq 1$ are physically relevant, and the transmitting states with $|\lambda| = 1$ need to be analyzed carefully to correctly identify which of those to include since only half of the $|\lambda| = 1$ are allowed.

Perturbation analysis for $|\lambda| = 1$ eigenvalues

Determining which $|\lambda| = 1$ get pushed into the unit circle is of vital importance for finding the proper surface Green's function. The starting point of the GSD is finding the unitary matrices Q and Z and the triangular matrices T and S such that [30]

$$Q^\dagger A Z = T, \quad (18)$$

$$Q^\dagger B Z = S, \quad (19)$$

which can be done using standard LAPACK routines, e.g., `zggcs`, or any other standard numerical packages. Using the definition of A_0 and $B = B_0$, we write

$$Q_0^\dagger A_0 Z_0 = T_0, \quad (20)$$

$$Q_0^\dagger B Z_0 = S_0, \quad (21)$$

which forms the starting point of our analysis. First we use the properties of unitary matrices $Q^\dagger = Q^{-1}$ and $Z^\dagger = Z^{-1}$, and we assume a small perturbation, i.e., we throw away all

η^2 terms. Defining

$$Q = Q_0 + \eta\delta Q, \quad (22)$$

we write

$$\begin{aligned} Q^\dagger Q &= (Q_0 + \eta\delta Q)^\dagger (Q_0 + \eta\delta Q) \\ &= Q_0^\dagger Q_0 + \eta[Q_0^\dagger \delta Q + (\delta Q)^\dagger Q_0] + O(\eta^2) \equiv I, \end{aligned} \quad (23)$$

$$\begin{aligned} QQ^\dagger &= (Q_0 + \eta\delta Q)(Q_0 + \eta\delta Q)^\dagger \\ &= Q_0 Q_0^\dagger + \eta[Q_0(\delta Q)^\dagger + \delta Q Q_0^\dagger] + O(\eta^2) \equiv I, \end{aligned} \quad (24)$$

which result in the conditions

$$Q_0^\dagger Q_0 = Q_0 Q_0^\dagger \equiv I, \quad (25)$$

$$Q_0^\dagger \delta Q + (\delta Q)^\dagger Q_0 \equiv 0. \quad (26)$$

This matrix equation in Eq. (26) is fulfilled when

$$\delta Q = iQ_0. \quad (27)$$

The same holds for the unitary matrix Z , so we get

$$Q = Q_0 + i\eta Q_0 = Q_0(1 + i\eta), \quad (28)$$

$$Z = Z_0 + i\eta Z_0 = Z_0(1 + i\eta). \quad (29)$$

Now going back to the GSD in Eq. (18) for A , we obtain

$$\begin{aligned} Q^\dagger AZ &= Q_0^\dagger(1 - i\eta)(A_0 + i\eta I_{22})Z_0(1 + i\eta) \\ &= T_0 + \eta\delta T, \end{aligned} \quad (30)$$

which gives the conditions

$$T_0 = Q_0^\dagger A_0 Z_0, \quad (31)$$

$$\delta T = iQ_0^\dagger I_{22} Z_0. \quad (32)$$

Correspondingly for the B equation, we obtain

$$\begin{aligned} Q^\dagger BZ &= Q_0^\dagger(1 - i\eta)BZ_0(1 + i\eta) \\ &= Q_0^\dagger BZ_0 \\ &= S_0 + \eta\delta S, \end{aligned} \quad (33)$$

which gives the condition

$$S_0 = Q_0^\dagger BZ_0, \quad (34)$$

$$\delta S = 0. \quad (35)$$

The eigenvalues of the original problem are given by the ratio [30]

$$\lambda_n = \frac{[T]_{n,n}}{[S]_{n,n}} \quad (36)$$

and for the $\eta = 0$ case

$$\lambda_n^0 = \frac{[T_0]_{n,n}}{[S_0]_{n,n}}. \quad (37)$$

Since $S = S_0$, we can write the eigenvalues in terms of the perturbation as

$$\lambda_n = \frac{[T_0 + \eta\delta T]_{n,n}}{[S_0]_{n,n}} = \frac{[T_0]_{n,n} + \eta[\delta T]_{n,n}}{[S_0]_{n,n}}, \quad (38)$$

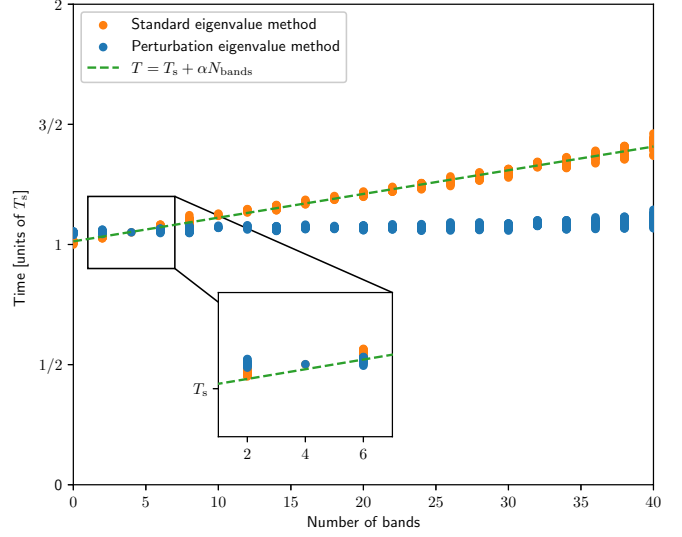


FIG. 3. Comparison of the time required to solve the graphene nanoribbon problem with the standard eigenvalue method and the perturbation eigenvalue method as a function of the number of conducting bands N_{bands} .

where $[\delta T]_{n,n} = [iQ_0^\dagger I_{22} Z_0]_{n,n}$. The eigenvalues on the unit circle need to be considered separately, i.e., which are moved inside the unit circle and which are not. The $|\lambda_n^0| = 1$ eigenvalues are modified in the presence of $i\eta$ such that their length is

$$|\lambda_n|^2 = \left| \frac{[T_0]_{n,n}}{[S_0]_{n,n}} \right|^2 \left| 1 + \eta \frac{[\delta T]_{n,n}}{[T_0]_{n,n}} \right|^2 \quad (39)$$

$$= 1 + 2\eta \mathcal{R} \left\{ \frac{[\delta T]_{n,n}}{[T_0]_{n,n}} \right\} + O(\eta^2). \quad (40)$$

Here the crux of the matter is that only the *sign* of the real part of $[\delta T]_{n,n}/[T_0]_{n,n}$ is needed, i.e., in determining which states will get pushed inside the unit circle and which will be pushed outside. This important point is the key result of our method, i.e., we can uniquely identify which $|\lambda_n| = 1$ eigenvalues get pushed into the unit circle without having either to calculate the mode velocity or to use η explicitly. Once the eigenvalues $|\lambda_0|^2 = 1$ are distinguished, the eigenvalues are rearranged and the Green's function can then simply be written as [see Eq. (3.44) in [18]]

$$GV^\dagger = Z_{11}^\dagger Z_{12}, \quad (41)$$

where the subspace 1 is determined by having $|\lambda_n| < 1$, and subspace 2 is determined by having $|\lambda_n| > 1$ [18]. Note that we never need η explicitly, we simply use $[\delta T]_{n,n}$ and $[T_0]_{n,n}$, which are independent of η [27].

We can compare this method with the standard method of choosing the propagating eigenvalues for the sign of the velocity. Let us define N_{sl} as the number points in a slice (see Fig. 4), N_{bands} as the number of propagating energy bands, and T_s as the number of operations for a full QZ factorization. The full QZ factorization takes $T_s = 66(2N_{\text{sl}})^3 = 66 \times 8N_{\text{sl}}^3$ [30].

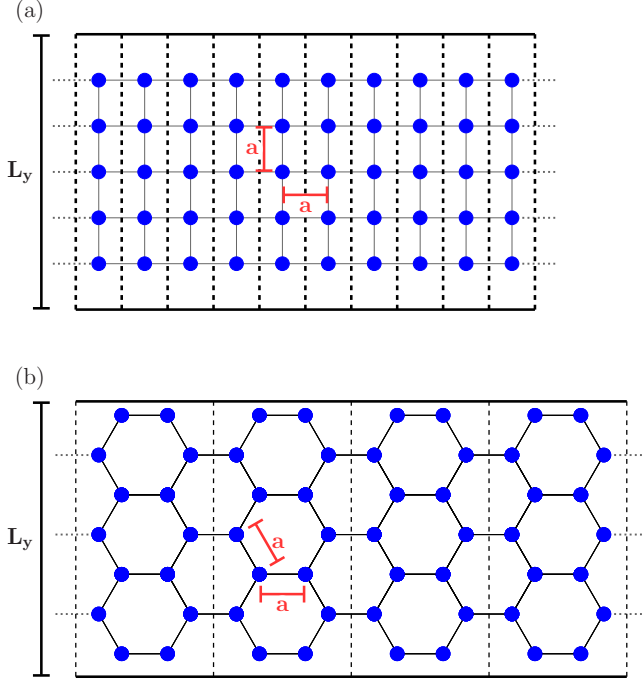


FIG. 4. Schematics that show how the wires are discretized and sliced. All slicings are along the y -direction. (a) The Rashba system is discretized on a regular rectangular grid and sliced in slices that are one grid point thick. (b) The graphene nanoribbon system is discretized on a hexagonal grid defining the graphene structure, and each slice is wide enough to contain one hexagon substructure.

Finding the velocity of a given mode takes

$$\left(\frac{2}{3}N_{sl}^3 \times 2_{[interaction]}\right)4_{[spin \times left+right]}N_{bands} = \frac{2N_{bands}}{3 \times 66}T_s = \alpha N_{bands}, \quad (42)$$

where at least two iterations are needed to find the eigenvalues [30], and $\frac{2}{3}N_{sl}^3$ operations are required to find the eigenvector of each mode. Note that to find the transmitting eigenvalues, the original Schrödinger equation can be solved, not the doubled problem in Eq. (14) [18]. Using Eq. (42), we can deduce that for $N_{bands} = 12$, the total computation time will increase by $\approx 10\%$, and for $N_{bands} = 50$ the computation time will increase by half. Figure 3 shows a comparison of the time required to compute the self-energy of the Rashba strip (described below) with the standard method and the perturbation method described above as a function of time. In the figure, we see that the time required for the standard method scales linearly with the number of propagating bands. From the estimate in Eq. (42), one obtains $\alpha^{est} = \frac{2}{3 \times 66}T_s \approx 0.010T_s$, and the numeric result is $\alpha^{num} \approx 0.0099T_s$. In contrast to the standard method, the time required for the perturbation method is constant with respect to the number of propagating bands. So once the number of propagating bands becomes substantial, relevant for, e.g., *ab initio* calculations [14], the computational cost of calculating the velocities with the standard method becomes quite costly compared to our method.

IV. RESULTS

In the following, we will make a comparison [38] of the two eigenvalue methods, which are described above, and the Lopez-Sancho method [9]. As explained above, with the eigenvalue method, Eq. (15) can be solved without explicitly adding to the energy the infinitesimal complex part η . This corresponds to using matrices A_0 and B_0 in Eqs. (16) and (17). However, turning η to zero can result in the regular eigenvalue method becoming unstable. This can be largely fixed by Schur-factorizing. More difficult instabilities in the eigenvalue calculations can be solved by reintroducing the infinitesimal complex part η . Often roughly one order of magnitude above the machine precision is enough. Note that in these difficult cases, a nonzero η is required in calculating the eigenvalues themselves. That is, they are not introduced to separate eigenvalues internal and external to the unit circle in the complex plane.

In our comparison, we will consider two cases of two-dimensional half-infinite quantum wires of width L_y . The first case is a wire with Rashba spin-orbit interaction [32,33]. The second case is a wire constructed out of graphene armchair nanoribbon [35,36]. Both systems are confined on the upper and lower y -axis boundary with an infinite hard-wall potential. Figure 4 shows how the wires are discretized and sliced into connected subsystems.

In both cases, the η is varied from 1.0×10^{-16} (lower than the machine epsilon) to 1.0×10^{-13} in steps of one order of magnitude. Note that this is done for all three methods even though it should not effect the reordering of eigenvalues for the perturbation eigenvalue method. For both systems, we use 98×98 H and V matrices. The form of the matrices H and V for the Rashba system is shown in Appendix C, and the corresponding form for the graphene nanoribbon system can be found in [36].

A. Rashba system

The first case that we consider is the calculation of self-energy for a half-infinite wire of 2D electron gas including a Rashba spin-orbit interaction corresponding to $k_R L_y = 1$, see Appendix C, with the number of transverse points $N_y = 49$ (which gives $N = 2N_y = 98$ due to spin). We use all three methods to calculate the self-energy over an energy range from $E = 0$ to $10E_0$ with an interval of $0.05E_0$ between energy points, where $E_0 = \hbar^2 \pi^2 / 2mL_y^2$ is the energy of the lowest transverse eigenstate, in the absence of Rashba interaction. Each method is repeated 10 times, and the minimum time required to calculate the self-energy is recorded for each energy value. We also record the backward error of the solution to Eq. (6) at each energy value for all the methods. The results are shown in Fig. 5, where we compare the results for all three methods—the perturbation eigenvalue method, the standard eigenvalue method, and the Lopez-Sancho method.

Figures 5(a), 5(b) and 5(c) show for reference the band structure of the system. For the range of energy that we use, there are three energy branches that correspond to the lowest three branches of transverse modes of the system. The Rashba field splits each branch into two energy bands. The time re-

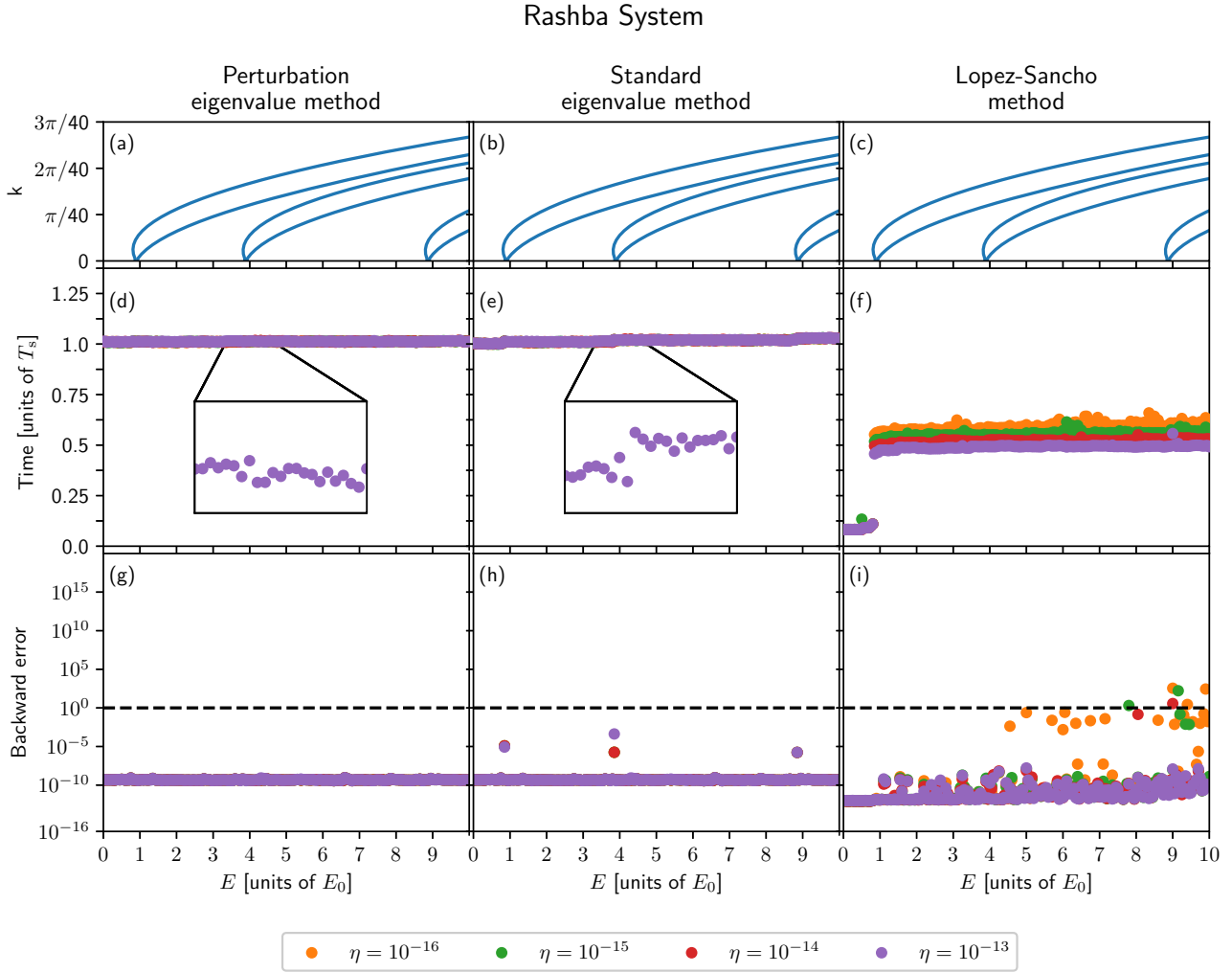


FIG. 5. Timing result and backward error as a function of energy for the Rashba system. The energy band of the system is shown for reference in (a), (b), and (c). The timing results are shown in (d) for the perturbation eigenvalue method, in (e) for the standard eigenvalue method, and in (f) for the Lopez-Sancho method. The backward error is shown in (g) for the perturbation eigenvalue method, (h) for the standard method, and (i) for the Lopez-Sancho method. The insets in (d) and (e) highlight the difference in calculation time of the eigenvalue methods at an opening of a new energy band.

quired to calculate the self-energy is shown in Figs. 5(d), 5(e) and 5(f) for the perturbation eigenvalue method, the standard eigenvalue method, and the Lopez-Sancho method, respectively. Here all times are scaled in T_s , which corresponds to the lowest value of time measured for the solution of the eigenvalue methods. In Figs. 5(d) and 5(e), the insets highlight the calculation time at an opening of a new energy band.

From Figs. 5(d) and 5(e) we see that the perturbation eigenvalue method and the standard eigenvalue method require overall roughly the same amount of time to calculate the self-energy of the system for this energy range. The perturbation eigenvalue method shows a negligible change in time required to calculate the self-energy as a function of energy. Upon close inspection [see the inset in Fig. 5(e)], the standard eigenvalue method shows a stepwise increase in time with energy. This step is repeated at the opening for each band. Overall, the step structure of the calculation time of the standard eigenvalue method starts by requiring slightly less time than the perturbation eigenvalue method when there are no energy bands open, but requiring more time with each

energy band that opens. This is because the calculation of the velocities involves diagonalizing a subspace that grows with the number of open energy bands. For this range of energy, the Lopez-Sancho method outperforms both eigenvalue methods. The time required for the Lopez-Sancho method to calculate the self-energy is roughly half that of the eigenvalue methods. The time is fairly stable within the energy range that contains open bands, but it increases slightly with lower values of η . However, the Lopez-Sancho method is not as stable as the eigenvalue methods. This can be seen in Figs. 5(g), 5(h) and 5(j), which show the backward error, a measure of how well the calculated solution fulfills the original equation, Eq. (4), for each method. Figures 5(g) and 5(h) show that both of the eigenvalue methods are very robust, producing solutions with roughly the same low amount of backward error over the whole energy range. However, the standard eigenvalue methods show an increase in backward error at the opening of new energy bands. This is not seen in the perturbation eigenvalue method, and it is due to diagonalizing near-zero velocity subspaces in the standard method that are close to

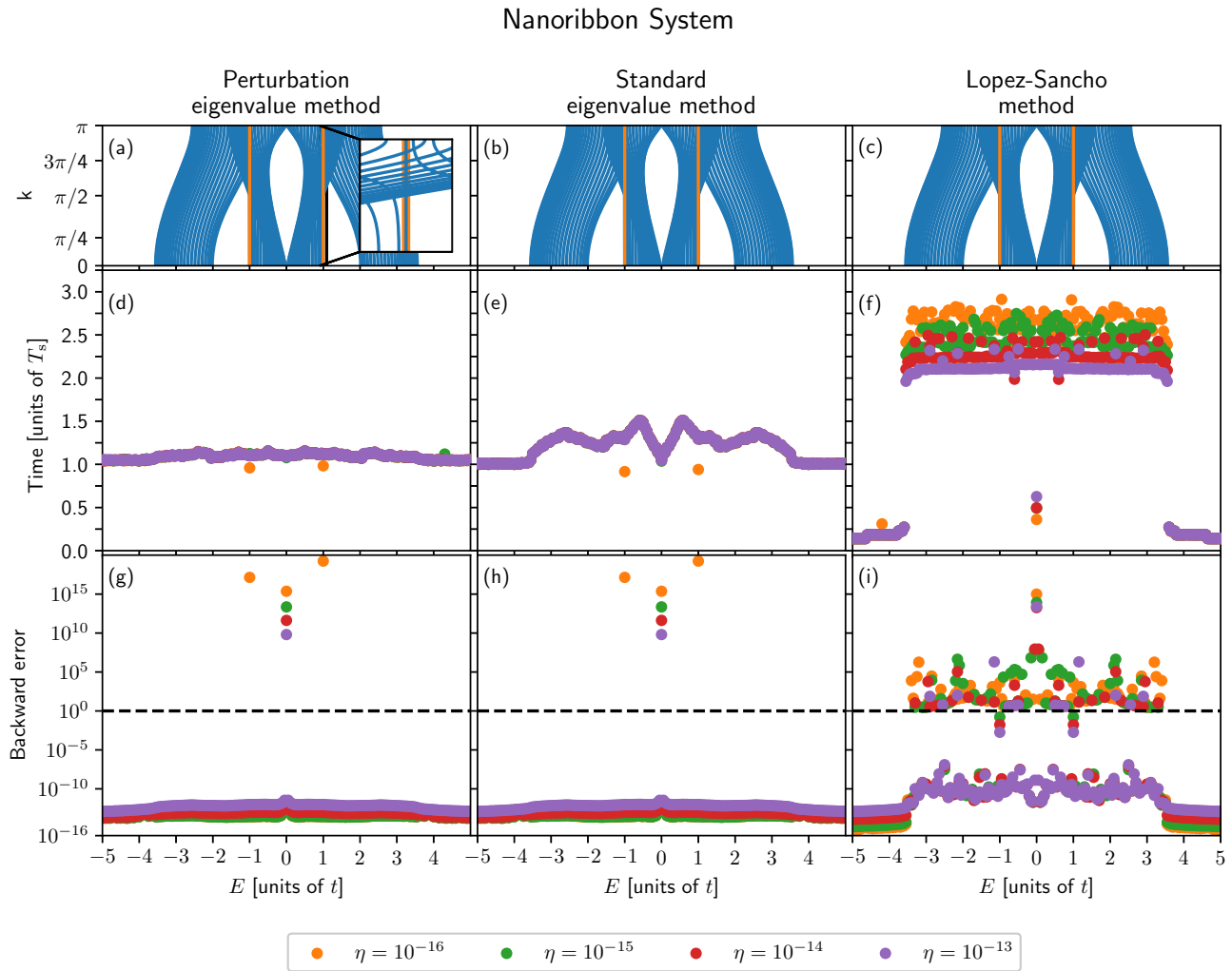


FIG. 6. Timing results and backward error as a function of energy for the graphene nanoribbon system. The energy band of the system is shown for reference in (a), (b), and (c). The timing results are shown in (d) for the perturbation eigenvalue method, in (e) for the standard eigenvalue method, and in (f) for the Lopez-Sancho method. The backward error is shown in (g) for the perturbation eigenvalue method, (h) for the standard eigenvalue method, and (i) for the Lopez-Sancho method.

being singular. In Fig. 5 we see that the backward error of the solutions produced by the Lopez-Sancho method has more fluctuations, and for some cases of low η values and high energies it gives wrong solutions (backward error close to or larger than 1).

B. Graphene nanoribbon system

Results from calculations of the self-energy of the graphene nanoribbon case are shown in Fig. 6. The self-energy of this system is calculated for energies ranging from $-5t$ to $5t$ with intervals of $0.05t$ between points, where t is the hopping integral. Figures 6(a), 6(b) and 6(c) show the energy bands of the system for reference. In Figs. 6(d), 6(e) and 6(f) we have the time required to calculate the self-energy with the perturbation eigenvalue method, the standard eigenvalue method, and the Lopez-Sancho method, respectively. Note that the time is scaled in time units T_s that correspond to the smallest calculation time for the eigenvalue methods.

The backward error of the solution to Eq. (6) produced by the perturbation eigenvalue method, the standard eigenvalue method, and the Lopez-Sancho method are shown in Figs. 6(g), 6(h) and 6(i), respectively.

We see in Fig. 6(g) that the time required to find the solution to Eq. (4) with the perturbation eigenvalue method is fairly stable over the whole energy range, remaining slightly above T_s . However, the time required for the standard eigenvalue method [see Fig. 6(h)] requires extra time proportional to the number of open energy bands [see Fig. 6(b)]. For this system, the Lopez-Sancho method is considerably slower, requiring, as seen in Fig. 6(i), about two to three times more calculation time. The solution time is also more scattered due to the fact that the Lopez-Sancho method is an iterative method.

The backward error of the two eigenvalue methods, seen in Figs. 6(g) and 6(h), is very low over the whole energy range except at energies $E = -1t, 0t, \text{ and } 1t$. This is due to the fact that the problem of finding eigenvalues is unstable at these points. At the $E = -1t$ and $+1t$ points, the energy bands form vertical structures, marked with orange in Figs. 6(a),

6(b) and 6(c) and shown in the inset in Fig. 6(a), resulting in the matrix $E-H$ becoming rank-deficient. The instabilities at energies $E = -1t$ and $+1t$ are resolved by adding η above machine epsilon. However, the instability at $E = 0$ persists but with lower backward error as η is increased.

In Fig. 6(i) we see that the backward error for the Lopez-Sancho method is larger than 10^0 orders of magnitude for many energy values with $\eta < 10^{-14}$ and a few energy values with $\eta < 10^{-13}$. Also for the Lopez-Sancho method, the solution for the energy values $E = -1t$, $E = 0t$, and $E = 1t$ seems to be unstable and is not fully solved with higher η at energy values $E = -1t$ and $1t$.

V. CONCLUSIONS

Here we presented an alternative method to calculate the surface Green's functions of infinite chains that are relevant for transport in nanostructures. Our method does not require finding the mode velocities, thus it saves computational time. The computational time required to find the mode velocities

increases linearly with the number of transmitting bands, which in the case of 50 modes leads to a 50% increase in computation time to find the surface Green's function. The present method circumvents the velocity-finding step leading to a *fixed* computational time irrespective of the number of transmitting modes. We presented an outline of the computational methods, and we also performed detailed numerical calculations comparing our method to the traditional velocity-finding method and the Lopez-Sancho algorithm. In terms of computation time and accuracy, the present method outperforms them both.

ACKNOWLEDGMENTS

This work was supported by the Reykjavik University Research Fund.

APPENDIX A: SURFACE GREEN'S FUNCTION

The full Green's function of the infinite chain is determined by the equation

$$\left(\begin{array}{c|ccc} (E - H_0) & -V_0 & 0 & \cdots \\ \hline -V_0^\dagger & E - H & V & 0 \\ 0 & -V^\dagger & (E - H) & \\ \vdots & 0 & & \ddots \end{array} \right) \left(\begin{array}{c|cc} G_{00} & G_{0,1} & G_{0,2} \\ \hline G_{1,0} & G_{1,1} & G_{1,2} \\ G_{2,0} & G_{2,1} & G_{2,2} \\ \vdots & & \ddots \end{array} \right) = \left(\begin{array}{c|cc} I & 0 & 0 \\ \hline 0 & I & 0 \\ 0 & 0 & I \\ & & \ddots \end{array} \right), \quad (\text{A1})$$

where the Hamiltonian matrix is block-tridiagonal. The vertical and horizontal lines indicate the submatrices for site $l = 0$ and sites $l > 0$ and the coupling between them, which is determined by V_0 . It is convenient to rewrite the above equation on a 2×2 form,

$$\left(\begin{array}{c|c} E - H_0 & -V \\ \hline -V^\dagger & E\mathbb{I} - \mathbb{H} \end{array} \right) \left(\begin{array}{c|c} G_{00} & \mathbb{G}_{0,c} \\ \hline \mathbb{G}_{c,0} & \mathbb{G}_c \end{array} \right) = \left(\begin{array}{c|c} I & \mathbb{O} \\ \hline \mathbb{O}^\dagger & \mathbb{I} \end{array} \right). \quad (\text{A2})$$

Writing out the equations corresponding to block matrix elements (1,1) and (2,1) results in the following two equations:

$$(E - H_0)G_{00}(E) - V\mathbb{G}_{c,0}(E) = I, \quad (\text{A3})$$

$$-V^\dagger G_{00}(E) + (E\mathbb{I} - \mathbb{H})\mathbb{G}_{c,0}(E) = \mathbb{O}^\dagger, \quad (\text{A4})$$

from which we obtain an equation for the Green's function of site $l = 0$,

$$(E - H_0)G_{00}(E) - (V(E\mathbb{I} - \mathbb{H})^{-1}V^\dagger)G_{00}(E) = I. \quad (\text{A5})$$

By definition, the Green's function of the $l > 0$ chain is given by $\mathbb{G}_c(E) = (E\mathbb{I} - \mathbb{H})^{-1}$. Due to the fact that only the $l = 1$ block of V is nonzero, the triple matrix product $V\mathbb{G}_cV^\dagger$ is also only nonzero in the $l = 1$ block,

$$[V\mathbb{G}_cV^\dagger]_{1,1} = V[\mathbb{G}_c]_{1,1}V^\dagger = VG_{1,1}V^\dagger. \quad (\text{A6})$$

Using Eq. (A6), we can rewrite Eq. (A5) as

$$((E - H_0) - (VG_{1,1}V^\dagger))G_{0,0} = I, \quad (\text{A7})$$

which is Eq. (1) in the main text.

After Eq. (4) is converted into the standard quadratic form, then the quantity that is obtained is GV^\dagger , which, after left-multiplying by V (in the case when $V = V_0$), results in Eq. (2) for the self-energy. If the Green's function itself is needed, then Eq. (3) gives the G directly, and it does not require an inversion of V .

APPENDIX B: INTERSITE GREEN'S FUNCTION

Having calculated $G_{0,0}V^\dagger = GV^\dagger$ via Eq. (6), all intersite Green's function elements $G_{n,0}$ can be subsequently calculated, starting from Eq. (A1) with $H_0 = H$. First, we look at column 1 and line 1 of Eq. (A1), which results in

$$(E - H)G_{0,0} - VG_{1,0} = \mathbb{I}, \quad (\text{B1})$$

which, after right-multiplying with V^\dagger , can be written as

$$VG_{1,0}V^\dagger = (E - H)G_{0,0}V^\dagger - V^\dagger \quad (\text{B2})$$

$$= (\mathbb{I} + VG_{1,1}V^\dagger G_{0,0})V^\dagger - V^\dagger \quad (\text{B3})$$

$$= V(G_{0,0}V^\dagger)^2. \quad (\text{B4})$$

In Eq. (B3), we used Eq. (6) to rewrite

$$(E - H)G_{0,0}V^\dagger = \mathbb{I} + V(G_{0,0}V^\dagger)^2. \quad (\text{B5})$$

Since V is arbitrary, Eq. (B4) implies that

$$G_{1,0}V^\dagger = (G_{0,0}V^\dagger)^2. \quad (\text{B6})$$

We now use induction to prove Eq. (8), i.e., that $G_{n,0}V^\dagger = (G_{0,0}V^\dagger)^{n+1}$, for $n \geq 1$. The condition is trivially satisfied for $n = 0$, and the equations leading to Eq. (B6) prove the $n = 1$

case. Right-multiplying by V^\dagger , the equation in column 1 and line $n + 1 > 1$ in Eq. (A1) results in

$$VG_{n+1,0}V^\dagger = -V^\dagger G_{n-1,0}V^\dagger + (E - H)G_{n,0}V^\dagger. \quad (\text{B7})$$

Inserting the inductive step for n and $n - 1$ on the right-hand side of the above equation results in

$$VG_{n+1,0}V^\dagger = -V^\dagger(G_{0,0}V^\dagger)^n + (E - H)(G_{0,0}V^\dagger)^{n+1} \quad (\text{B8})$$

$$= -V^\dagger(G_{0,0}V^\dagger)^n + [V^\dagger + V(G_{0,0}V^\dagger)^2](G_{0,0}V^\dagger)^n \quad (\text{B9})$$

$$= V(G_{0,0}V^\dagger)^2(G_{0,0}V^\dagger)^n \quad (\text{B10})$$

$$= V(G_{0,0}V^\dagger)^{n+2}, \quad (\text{B11})$$

which completes the proof, since V is arbitrary.

APPENDIX C: FORM OF H_{sl} AND V_{sl} FOR THE RASHBA SYSTEM

The Rashba spin-orbit interaction in a 2D electron system is described by the following Hamiltonian operator:

$$H_R = -\frac{\hbar^2}{2m} \left(\frac{\partial^2}{\partial x^2} + \frac{\partial^2}{\partial y^2} \right) \sigma_0 + \frac{\alpha}{i} \left(\frac{\partial}{\partial x} \sigma_y - \frac{\partial}{\partial y} \sigma_x \right), \quad (\text{C1})$$

where \hbar is the Planck constant, m is the electron effective mass, and α is the Rashba constant, which characterizes the strength of the spin-orbit coupling. The 2×2 spin structure is determined by the standard Pauli matrices σ_0 , σ_x , and σ_y . Assuming a hard-wall confinement in the y -direction [see Fig. 4(a)], the number of lattice points N_y determines the

lattice parameter

$$a = \frac{L_y}{N_y + 1}. \quad (\text{C2})$$

Using centered finite-difference relations (three-point stencil for the second derivative and two-point stencil for the first derivatives), the matrices H_{sl} and V_{sl} take the following form:

$$H_{sl} = E_0 \begin{pmatrix} d & b & 0 & & & \\ b^\dagger & d & b & 0 & & \\ 0 & b^\dagger & d & b & 0 & \\ & & & \ddots & & \\ & & 0 & b^\dagger & d & b \\ & & & & 0 & b^\dagger & d \end{pmatrix}, \quad (\text{C3})$$

$$V_{sl} = E_0 \begin{pmatrix} c & 0 & 0 & & & \\ 0 & c & 0 & 0 & & \\ 0 & 0 & c & 0 & 0 & \\ & & & \ddots & & \\ & & 0 & 0 & c & 0 \\ & & & & 0 & 0 & c \end{pmatrix}, \quad (\text{C4})$$

where the 2×2 block matrices d , b , and c are defined as

$$d = 4 \frac{(N_y + 1)^2}{\pi^2} \sigma_0, \quad (\text{C5})$$

$$b = -\frac{(N_y + 1)^2}{\pi^2} \sigma_0 + i \frac{L_y k_R}{\pi^2} (N_y + 1) \sigma_x, \quad (\text{C6})$$

$$c = -\frac{(N_y + 1)^2}{\pi^2} \sigma_0 - i \frac{L_y k_R}{\pi^2} (N_y + 1) \sigma_y, \quad (\text{C7})$$

where $k_R = \frac{m\alpha}{\hbar^2}$ is the so-called the spin-orbit wave number, so that $L_y k_R$ is a dimensionless parameter. The energy parameter is given by $E_0 = \frac{\hbar^2 \pi^2}{2mL_y^2}$.

-
- [1] D. K. Ferry and S. M. Goodnick, *Transport in Nanostructures*, edited by H. Ahmed, M. Pepper, and A. Broers (Cambridge University Press, Cambridge, 1997).
- [2] S. Datta, *Electronic Transport in Mesoscopic Systems* (Cambridge University Press, Cambridge, 1995).
- [3] C. Cohen-Tannoudji, B. Diu, and F. Laloë, *Quantum Mechanics* (Wiley, New York, 1977).
- [4] Y. Blanter and M. Büttiker, *Phys. Rep.* **336**, 1 (2000).
- [5] Y. V. Nazarov, *Handbook of Theoretical and Computational Nanotechnology* (American Scientific, Valencia, CA, 2006), Chap. 95, pp. 1–83.
- [6] G. Hackenbroich, *Phys. Rep.* **343**, 463 (2001).
- [7] M. Bravi, R. Farchioni, G. Grosso, and G. Pastori Parravicini, *Phys. Rev. B* **90**, 155445 (2014).
- [8] N. M. Peres, *Eur. Phys. J. B* **72**, 183 (2009).
- [9] M. P. Lopez Sancho, J. M. Lopez Sancho, J. M. L. Sancho, and J. Rubio, *J. Phys. F* **15**, 851 (1985).
- [10] T. Ando, *Phys. Rev. B* **44**, 8017 (1991).
- [11] X.-G. Zhang and A. Gonis, *Phys. Rev. Lett.* **62**, 1161 (1989).
- [12] A. Gonis, *Phys. Rev. B* **34**, 8313 (1986).
- [13] K. S. Dy, S.-Y. Wu, and T. Spratlin, *Phys. Rev. B* **20**, 4237 (1979).
- [14] S. Sanvito, C. J. Lambert, J. H. Jefferson, and A. M. Bratkovsky, *Phys. Rev. B* **59**, 11936 (1999).
- [15] J. Taylor, H. Guo, and J. Wang, *Phys. Rev. B* **63**, 245407 (2001).
- [16] A. R. Rocha, V. M. García-Suárez, S. Bailey, C. Lambert, J. Ferrer, and S. Sanvito, *Phys. Rev. B* **73**, 085414 (2006).
- [17] I. Rungger and S. Sanvito, *Phys. Rev. B* **78**, 035407 (2008).
- [18] M. Wimmer, Ph.D. thesis, Universität Regensburg, 2008.
- [19] H. H. B. Sørensen, P. C. Hansen, D. E. Petersen, S. Skelboe, and K. Stokbro, *Phys. Rev. B* **77**, 155301 (2008).
- [20] M. Farmanbar, T. Amlaki, and G. Brocks, *Phys. Rev. B* **93**, 205444 (2016).
- [21] S.-H. Zhang, W. Yang, and K. Chang, *Phys. Rev. B* **95**, 075421 (2017).
- [22] H. Boumrrar, M. Hamidi, H. Zenia, and S. Lounis, *J. Phys.: Condens. Matter* **32**, 355302 (2020).
- [23] H. Ness, I. A. Sadovskyy, A. E. Antipov, M. van Schilfgaarde, and R. Lutchyn, *npj Comput. Mater.* **8**, 23 (2022).

- [24] H. Geng, J. Y. Wei, M. H. Zou, L. Sheng, W. Chen, and D. Y. Xing, *Phys. Rev. B* **107**, 035306 (2023).
- [25] M. Zwierzycki, P. A. Khomyakov, A. A. Starikov, K. Xia, M. Talanana, P. X. Xu, V. M. Karpan, I. Marushchenko, I. Turek, G. E. W. Bauer, G. Brocks, and P. J. Kelly, *Phys. Status Solidi B* **245**, 623 (2008).
- [26] P. A. Khomyakov, G. Brocks, V. Karpan, M. Zwierzycki, and P. J. Kelly, *Phys. Rev. B* **72**, 035450 (2005).
- [27] A. Umerski, *Phys. Rev. B* **55**, 5266 (1997).
- [28] T. P. Santos, L. R. Lima, and C. H. Lewenkopf, *J. Comput. Phys.* **394**, 440 (2019).
- [29] C. Groth, M. Wimmer, A. Akhmerov, and X. Waintal, *New J. Phys.* **16**, 063065 (2014).
- [30] G. Golub and C. F. van Loan, *Matrix Computations*, 4th ed. (The Johns Hopkins University Press, Baltimore, MD, 2013).
- [31] W. Roth, *Trans. Am. Math. Soc.* **32**, 61 (1930).
- [32] G. Thorgilsson and S. I. Erlingsson, *Phys. Rev. B* **82**, 245308 (2010).
- [33] B. K. Nikolić and S. Souma, *Phys. Rev. B* **71**, 195328 (2005).
- [34] J. Stoer and R. Bulirsch, *Introduction to Numerical Analysis*, Texts in Applied Mathematics (Springer, New York, 2002).
- [35] M. Wimmer, I. Adagideli, S. Berber, D. Tománek, and K. Richter, *Phys. Rev. Lett.* **100**, 177207 (2008).
- [36] C. H. Lewenkopf and E. R. Mucciolo, *J. Comput. Electron.* **12**, 203 (2013).
- [37] J. Bezanson, A. Edelman, S. Karpinski, and V. B. Shah, *SIAM Review* **59**, 6598 (2017).
- [38] All calculations in this paper were performed using the Julia computer language [37] and the code is stored in a github repository <https://github.com/gunnarth/Lead-Green-s-functions-from-quadratic-eigenvalue-problems-without-mode-velocity-calculations>.